Three-level ANPC Inverter Common-mode Voltage Analytical Characterization

Yang Huang
Department of Electrical Engineering and Computer Science
University of Tennessee
Knoxville, TN, USA, 37996
yhuang65@vols.utk.edu

Xin Xia
Department of Electrical Engineering and Computer Science
University of Tennessee
Knoxville, TN, USA, 37996
xxia6@vols.utk.edu

Hua (Kevin) Bai
Department of Electrical Engineering and Computer Science
University of Tennessee
Knoxville, TN, USA, 37996
hbai2@utk.edu

Fanning Jin
Mercedes Benz Research and Development Center
Mercedes Benz North America
Redford, MI, USA, 48239
fanning.jin@daimler.com

Xiaodong Shi
Mercedes Benz Research and Development Center
Mercedes Benz North America
Redford, MI, USA, 48239
xiaodong.shi@daimler.com

Bing Cheng
Mercedes Benz Research and Development Center
Mercedes Benz North America
Redford, MI, USA, 48239
bing.cheng@daimler.com

2022 IEEE 9th Workshop on Wide Bandgap Power Devices & Applications (WiPDA) | 978-1-6654-8900-3/22/$31.00 ©2022 IEEE | DOI: 10.1109/WiPDA56483.2022.9955294

***Abstract*—Evident in previous literature, in the motor drive system, the research on the analytical models for common-mode (CM) performance evaluation is inadequate but needed. Especially for the 3-level inverter system. The majority of work focuses on simulations and experiments. In this paper, an analytical model of CM voltage (CMV) in a 3-level inverter is presented based on Double Fourier Integral (DFI). The model could be extended to different 3-level modulation schemes such as conventional space vector PWM (CSVM), nearest three space vectors modulation (NTSVM), and reduced common-mode voltage modulation (RCMVM). The impact of these three modulation schemes on the CMV is comprehensively compared across varying modulation indices. An 800V/50kW 3L inverter will be built using off-the-shelf automotive-qualified 650V/60A GaN HEMTs from GaN Systems.**

Keywords—common-mode voltage, three-level inverter, space vector modulation

I. INTRODUCTION

Recently, high voltage batteries became popular in EVs because of the benefit of fast charging, longer mileage, and lower loss. In [1], a comparison has been made between multiple EVs and traditional petrol-driven vehicles in terms of inter-city travel. To have comparable travel time as petrol-driven vehicles, it is required to have a charger power of higher than 400 kW. With extreme fast charging techniques, the output voltage should be at least 800 V [2]. The high DC-link voltage not only enables the extremely fast charging but also leads to a smaller motor current for higher efficiency and smaller cables [3]. This requires either the device to have high voltage blocking capability, or the inverter to be multiple levels, such as a 3-level (3L) neutral point clamped inverter (NPCI) and active neutral point clamped inverter (ANPCI). Considering the cost, using lower voltage blocking devices in the multilevel inverter is more preferred, which not only lowers the device voltage stress but also enhances the output power quality because of the increase in voltage levels. GaN device has the merits of small package and high current capability, which is a perfect candidate for 3-level (3L) application. However, as the battery voltage increases, the motor drive system also suffers the increased common-mode voltage (CMV). In addition, the GaN device enables a higher switching frequency, thereby potentially higher CM current (CMC).

The CMV is generated through modulation and switching actions, hence, there is a possibility that by properly assigning the space vector combinations, the CMV can be reduced [4-6]. Reference [7] has validated this concept to achieve zero CMV generation with only 7 vectors, however, the maximum modulation index (MI) is reduced to 86.6% of the conventional SVM for the 2-level inverter, and the neutral point balancing issue will appear as these vectors are middle-length vectors. Therefore, CMV elimination is not the practical goal in the 3L system. As there are multiple 3L modulation schemes, each causes different CM performance, a proper model for the CMV evaluation is important. In [8-11], the double Fourier integral (DFI) method is used to model the CMV in a 2-level (2L) drive system, which shows excellent accuracy in CM profile prediction. However, few have been validated in the 3L system.

In this paper, a three-level ANPCI CMV modeling work for different 3L modulation schemes will be presented. The analytical model offers an approach to mathematically calculate the CM performance for a specific modulation method. Such an analytical model provides us with a powerful tool, allowing a comprehensive vision for further evaluations. Compared to the traditional simulation approach, the proposed analytical model could help designers to summarize the principle of CMV effectively. The analytical result of CMV could be coupled with the CM impedance, thereby conducting the CMC. The impact of all other variables, such as motor and controller parameters, could be actively evaluated through analytical equations instead of repeating the simulation.

II. Three-Level Inverter CMV Modeling

An ANPCI topology is shown in Fig. 1, compared with a two-level system, a three-level system alleviates the common-mode noise by providing more vector redundancy, and some vector combinations even null the CMV. The phase output voltage of a three-level inverter has 3 voltage levels ($V_{dc}/2$, 0, $-V_{dc}/2$). One conventional modulation method is, to use space vector modulation waveform to compare with the level-shifted carriers to generate the high-frequency PWM. The modulation mechanism is shown in Fig. 2.

$$V_{CM} = \frac{\left(V_{ao} + V_{bo} + V_{co}\right)}{3} \tag{1}$$

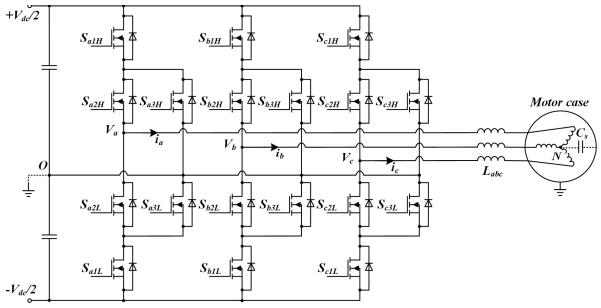

Fig. 1. Three-level ANPC inverter motor drive system

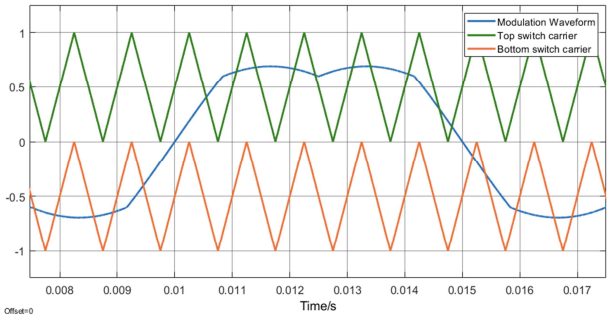

Fig. 2. 3L-ANPC CSVM modulation waveform

It is essential to use a low-frequency modulation waveform to compare with a high-frequency carrier waveform in any PWM method. The phase leg outputs a series of pulses switching between upper and lower DC bus, which not only have the fundamental component but also incorporate a series of unwanted harmonics due to switching processes. This indicates that based on the modulation waveform and carrier frequency, the output voltage spectrum could be predicted analytically. In some literature, the CMV analytical model for two-level inverters for various modulation schemes is proposed, however, for three-level inverters, the related modeling work is inadequate, the modeling complexity does exist, but a high integrated modeling approach could save the effort and extended to various three-level modulation methods.

DFI analysis is a mathematical tool that can provide analytical solutions to precisely identify harmonic components of a PWM signal. In inverter applications, assume the target function $f(t)$ is the voltage between the middle point of the phase leg and the middle point of the DC bus. $f(t)$ is a cyclic signal related to both $x(t)$ and $y(t)$ with period=2π. Here, $x(t)=\omega_s t+\theta_s$ and $y(t)=\omega_0 t+\theta_0$, representing the time variation of the high-frequency modulating wave and low-frequency modulated wave, respectively. By doing the DFI analysis on the PWM waveform, $f(t)$ can be expanded as (2). Where m is the carrier index variable, and n is the baseband index variable.

$$\begin{aligned} f(x,y) = {} & \frac{A_{00}}{2} + \sum_{n=1}^{\infty}\left\{A_{0n}\cos\left(n\left(\omega_0 t+\theta_0\right)\right)+B_{0n}\sin\left(n\left(\omega_0 t+\theta_0\right)\right)\right\} \\ & + \sum_{m=1}^{\infty}\left\{A_{m0}\cos\left(m\left(\omega_s t+\theta_s\right)\right)+B_{m0}\sin\left(m\left(\omega_s t+\theta_s\right)\right)\right\} \\ & + \sum_{m=1}^{\infty}\sum_{n=-\infty,\,n\neq 0}^{\infty}\left\{A_{mn}\cos\left(m\left(\omega_s t+\theta_s\right)+n\left(\omega_0 t+\theta_0\right)\right)+B_{mn}\sin\left(m\left(\omega_s t+\theta_s\right)+n\left(\omega_0 t+\theta_0\right)\right)\right\} \end{aligned} \tag{2}$$

A. Conventional Space Vector Modulation (CSVM)

According to the switching profile of CSVM in 3L-ANPC, the corresponding DFI integral bounds can be derived, as shown in Fig. 3. There are 8 sections for each fundamental cycle. Especially, in sections 1, 2, 5, and 6, there are three integration areas. In sections 3, 4, 7, and 8, there is only one (ignore the area where the pole voltage is 0). For instance, in section 1, the integration segments should be ($-\pi$, 1-), (1-, 1+), and (1+, π). The DFI math model (3) for CSVM in a 3L-ANPC is then generated from (2). Substituting different values for m and n, the carrier harmonics and sideband components of the CMV can be calculated and compared to the simulation.

The DFI model for CSVM in a 3L-ANPC is then generated from (6.1). Using (4.5)~(4.6) and substituting different values for m and n, the carrier harmonics and sideband components of the CMV can be calculated and compared to the simulation at f_0=100 Hz, f_s=10 kHz, 200V DC bus voltage, and 0.8 modulation index. As shown in Fig. 4, the calculated carrier harmonics and the sideband component of both phase voltage and CMV are very close to the simulation. Here only the $f_s \pm 15 f_0$ sideband harmonics around f_s are plotted. Therefore, the proposed analytical approach for CMV can be extended to multilevel scenarios.

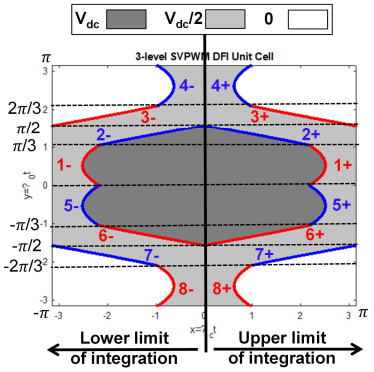

Fig. 3. DFI integral bounds for CSVM in a 3L-ANPC inverter

$$A_{mn}+jB_{mn}=\frac{1}{2\pi}\int_{-\pi}^{\pi}\int_{\substack{lowerlimit\\ insectori}}^{\substack{upperlimit\\ insectori}} Ue^{j(mx+ny)}dxdy$$

$$=\int_{-\pi}^{-\frac{2\pi}{3}}\int_{8-}^{8+}\frac{V_{dc}}{2}e^{j(mx+ny)}V_{dc}dxdy+\int_{-\frac{2\pi}{3}}^{-\frac{\pi}{3}}\int_{7-}^{7+}\frac{V_{dc}}{2}e^{j(mx+ny)}V_{dc}dxdy$$

$$+\int_{-\frac{\pi}{3}}^{-\frac{\pi}{2}}\int_{-\pi}^{6-}\frac{V_{dc}}{2}e^{j(mx+ny)}V_{dc}dxdy+\int_{-\frac{\pi}{3}}^{-\frac{\pi}{2}}\int_{6-}^{6+}V_{dc}e^{j(mx+ny)}V_{dc}dxdy+\int_{-\frac{\pi}{3}}^{-\frac{\pi}{2}}\int_{6+}^{\pi}\frac{V_{dc}}{2}e^{j(mx+ny)}V_{dc}dxdy$$

$$+\int_{-\frac{\pi}{3}}^{-\frac{\pi}{2}}\int_{-\pi}^{5-}\frac{V_{dc}}{2}e^{j(mx+ny)}V_{dc}dxdy+\int_{-\frac{\pi}{3}}^{-\frac{\pi}{2}}\int_{5-}^{5+}V_{dc}e^{j(mx+ny)}V_{dc}dxdy+\int_{-\frac{\pi}{3}}^{-\frac{\pi}{2}}\int_{5+}^{\pi}\frac{V_{dc}}{2}e^{j(mx+ny)}V_{dc}dxdy$$

$$+\int_{-\frac{\pi}{3}}^{-\frac{\pi}{2}}\int_{-\pi}^{1-}\frac{V_{dc}}{2}e^{j(mx+ny)}V_{dc}dxdy+\int_{-\frac{\pi}{3}}^{-\frac{\pi}{2}}\int_{1-}^{1+}V_{dc}e^{j(mx+ny)}V_{dc}dxdy+\int_{-\frac{\pi}{3}}^{-\frac{\pi}{2}}\int_{1+}^{\pi}\frac{V_{dc}}{2}e^{j(mx+ny)}V_{dc}dxdy$$

$$+\int_{-\frac{\pi}{3}}^{-\frac{\pi}{2}}\int_{-\pi}^{2-}\frac{V_{dc}}{2}e^{j(mx+ny)}V_{dc}dxdy+\int_{-\frac{\pi}{3}}^{-\frac{\pi}{2}}\int_{12-}^{2+}V_{dc}e^{j(mx+ny)}V_{dc}dxdy+\int_{-\frac{\pi}{3}}^{-\frac{\pi}{2}}\int_{2+}^{\pi}\frac{V_{dc}}{2}e^{j(mx+ny)}V_{dc}dxdy$$

$$+\int_{-\pi}^{-\frac{2\pi}{3}}\int_{3-}^{3+}\frac{V_{dc}}{2}e^{j(mx+ny)}V_{dc}dxdy+\int_{-\frac{2\pi}{3}}^{-\frac{\pi}{2}}\int_{4-}^{4+}\frac{V_{dc}}{2}e^{j(mx+ny)}V_{dc}dxdy \quad (3)$$

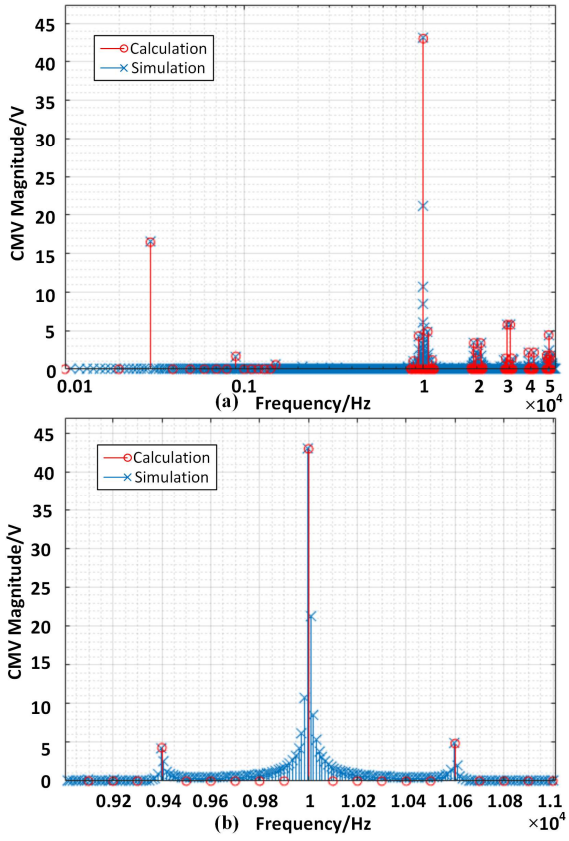

Fig. 4. Comparison of DFI result and simulation for 3L-ANPC inverter.

(a) Wide frequency range, (b) Zoomed-in view @f_s.

B. *Nearest Three Space Vectors Modulation (NTSVM)*

Direct CSVM modulation does not consider the modulation from the vector assignment point of view. However, determining the switching states, and the corresponding vector duration time is critical to synthesize the reference voltage vector [12]. As the total switching states count of a multilevel converter shows a cubic increase with the converter levels, the computational effort for the CSVM overwhelms quickly and is not preferred to be used for multilevel converters. Instead, using the nearest three vectors to synthesize the reference voltage is arguably the best approach as it saves the computation resources and forms precise vector decomposition. This modulation scheme is called nearest three vector modulation (NTSVM).

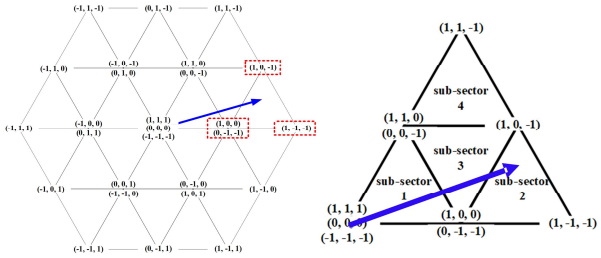

Fig. 5. NTSVM vector plane and reference synthesis.

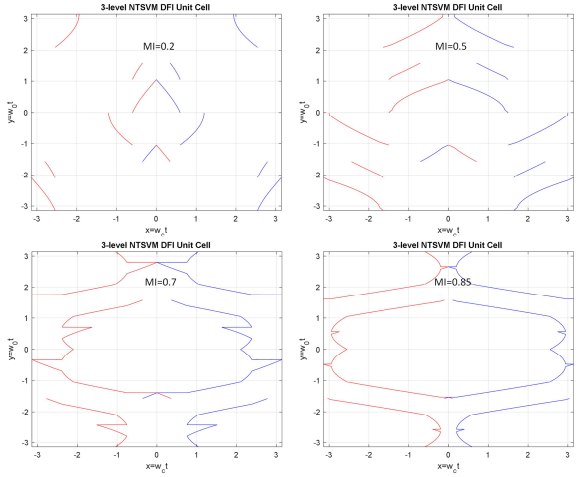

Fig. 6. DFI integral bounds for NTSVM in a 3L-ANPC inverter.

The NTSVM mechanism is illustrated in Fig. 5. Where the reference vector (blue) locates in sector-1 and subsector-2, the NTSVM requires to use the vectors on the three vertices of the subsector-2 triangle. Different from CSVM, which has a simplified modulation waveform that could be directly extended from a 2-level inverter, the modulation waveform of NTSVM is very complicated because of the subsector alternation. Depending on the modulation index, the modulation waveform shows a very different profile. The DFI bounds could be derived and plotted as shown in Fig. 6. Following the same steps that were applied in section 6.2.1, the analytical CMV spectrum vs the simulation result could be obtained. Fig. 7 shows the comparison given DC bus voltage = 800 V, MI=0.8, f_s=10 kHz and f_0=100 Hz. In Fig. 8, the peak CMV at the switching frequency point at different modulation indices is estimated and compared with the simulation. The result shows very accurate CMV prediction performance for NTSVM.

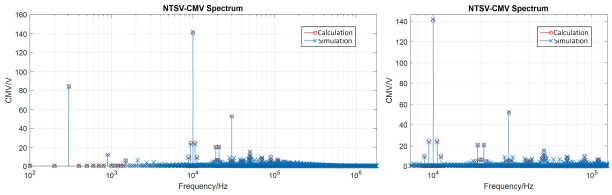

Fig. 7. Comparison of DFI result and simulation for 3L-NTSVM.

Left: Wide frequency range, Right: Zoomed-in around f_s.

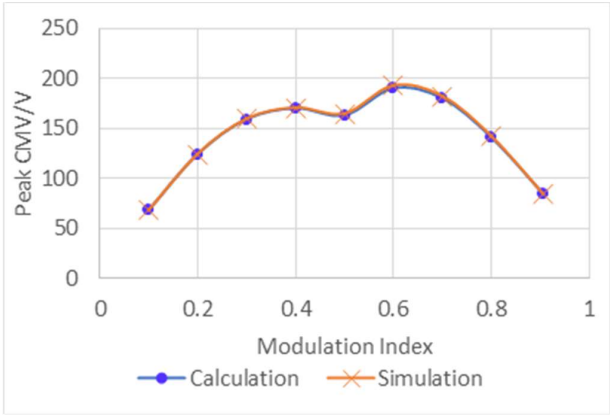

Fig. 8. Comparison of DFI result and simulation for 3L-NTSVM CMV peak @f_s.

C. *Reduced-CMV Modulation (RCMVM)*

NTSVM alternates the space vectors based on the minimum switching action principle to save the switching loss. However, some of the vectors will result in CMV higher than Vdc/6. Therefore, by avoiding using the 8 voltage vectors that generate $V_{dc}/6$ CMV, the system CMV could be constrained within $V_{dc}/6$. These 8 vectors are marked in Fig. 9. Other than that, the vector synthesis mechanism is the same as NTSVM. Due to the forced forbidden of some vectors, which means the 8 redundant switching states will not be used during modulation, the minimum switching action mechanism could not be realized. For example, in NTSVM sub-sector 2, the vector sequence minimum switching action would be (1, 0, 0), (1, 0, -1), (1, -1, -1) (0, -1, -1). However, in RCMVM sub-sector 2, the (0, -1, -1) vector is banned because it generates $V_{dc}/2$ CMV, the switching sequence becomes (1, 0, 0), (1, 0, -1), (1, -1, -1) (1, 0, 0). The last state transition includes an extra switching. Therefore, compared with NTSVM, the switching loss of RCMVM will be increased.

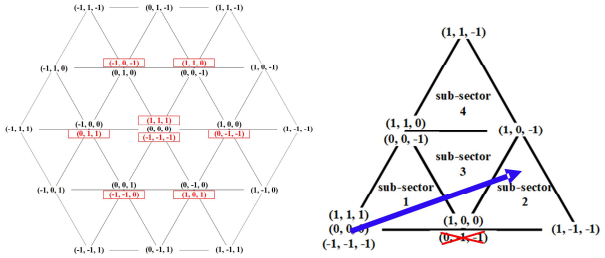

Fig. 9. RCMVM vector plane and reference synthesis.

Similar to NTSVM, the modulation waveform of RCMVM is also complicated compared with CSVM. The DFI bounds could be derived and plotted as shown in Fig. 10. The analytical CMV spectrum vs the simulation result could be obtained through the CMV spectrum estimation model. Fig. 11 shows the comparison given DC bus voltage = 800 V, MI=0.8, f_S=10 kHz and f_0=100 Hz. In Fig. 12, the peak CMV at the switching frequency point at different modulation indices is estimated and compared with the simulation. The result shows very accurate CMV prediction performance for RCMVM.

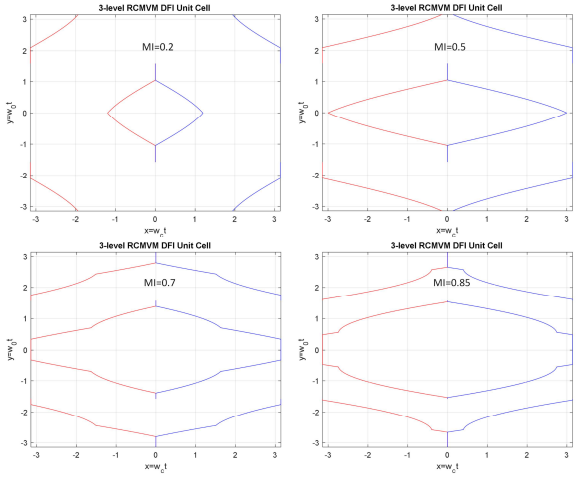

Fig. 10. DFI integral bounds for RCMVM in a 3L-ANPC inverter.

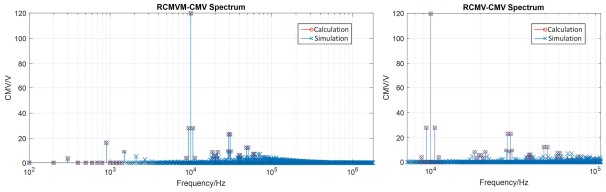

Fig. 11. Comparison of DFI result and simulation for 3L-RCMVM.

Left: Wide frequency range, Right: Zoomed-in around f_s.

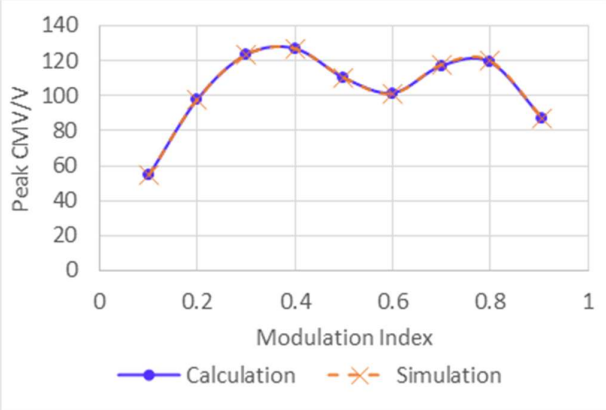

Fig. 12. Comparison of DFI result and simulation for 3L-RCMVM CMV peak @f_s.

III. Experimental Validation

To validate the 3-level modulation performance, a water-cooled 50 kW rated GaN-based 3-level inverter is built. The GaN HEMTs are from GaN System, GS66516T (650 V, 60 A). 3 pieces are paralleled at each switching position. The switching frequency is set to 10 kHz which is controlled by the FPGA, and the DC-link voltage is designed to undertake at most 800 V for high voltage applications. The prototype is shown in Fig. 13. The inverter is a stacked system with the bottom board carrying the power devices and the top board for the DC-link capacitors and input/output interfaces. The whole system sits on a copper grounding plate, where the inverter heatsink and motor case are solidly grounded.

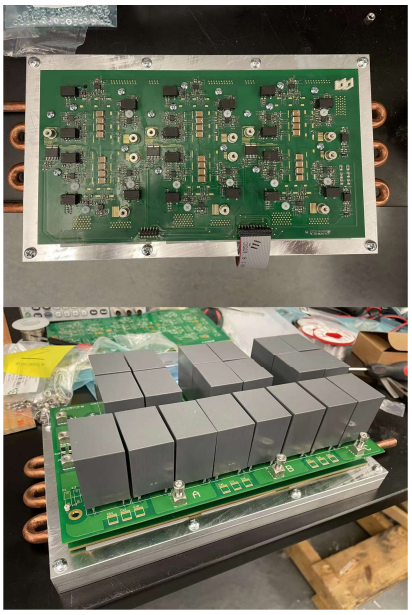

Fig. 13. Three-level GaN-based ANPC inverter prototype.

Top: Top view, Bottom: Final assembly.

Considering the frequency range of the prediction is low, the CMV spectrum components can be considered as linear to the DC input voltage. Therefore, a preliminary 200 V test result scaled up by 4 times can be used to emulate the 800 V performance on the low-frequency spectrum and will be used to compare with the 800 V simulation result to validate its prediction feasibility. Use the controller to implement three different 3L modulation schemes to sample the CMV data spectrum and compare it with the model estimation. Take CSVM CMV spectrum @*MI*=0.5 as an example, as shown in Fig 14, the spectrum of the prediction result on each harmonic point meets the tested spectrum. The complete prediction accuracy is shown in Fig. 15. For all three PWMs, the prediction results match the experimental results perfectly. This shows a promising accuracy of the potential software integration for an online prediction, which could collaborate with some dynamic modulation scheme switching algorithms. The real 800 V test and comparison will be the priority of the future work, before the prototype passed all voltage and power targets.

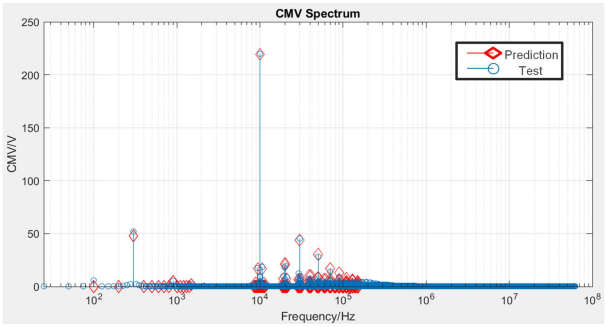

Fig. 14. Comparison of CMV spectrum between experimental result and prediction result for 3L-CSVM @*MI*=0.5. The "test" spectrum is generated based on a 200 V experiment result with 4-time amplification.

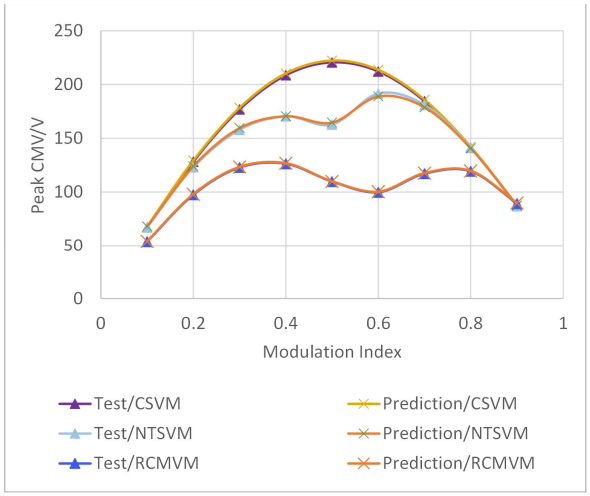

Fig. 15. Comparison of CMV spectrum peak value between experimental result and prediction result. The "test" data points are calculated based on a 200 V experiment result with 4-time amplification.

IV. Conclusion

The GaN-based multi-level topology could benefit the EV application under a high-voltage scenario from both power density and efficiency aspects. To overcome the CMV issue that is strengthened by the high voltage and high switching frequency that are introduced by the GaN device implementation, proper CM modeling is needed, which is less studied in past research work. This paper successfully extended the proposed CMV prediction model to the 3-level inverter. With NTSVM and RCMVM, though the modulation waveforms are complex, the suggested CMV prediction procedure with DFI still applies. The computation result matches the simulation result very accurately under current test condition. For the future work, a validation of the model with 800 V test result is planned. With the model being built, another future work is trying to integrate it into an online computation algorithm to dynamically switch modulation schemes according to the system operating point. This also needs differential-mode modeling to characterize the differential-model performance of various PWMs in the three-level inverter, a more comprehensive modeling work is required.

Acknowledgment

Authors would like to thank the support of Mercedes-Benz R&D North America. The experimental validation made use of the Engineering Research Center Shared Facilities supported by the Engineering Research Center Program of the National Science Foundation and DOE and the CURENT Industry Partnership Program.

References

[1] Meintz, Andrew, et al. "Enabling fast charging–Vehicle considerations." *Journal of Power Sources* 367 (2017): 216-227.

[2] Ronanki, Deepak, Apoorva Kelkar, and Sheldon S. Williamson. "Extreme fast charging technology—Prospects to enhance sustainable electric transportation." *Energies* 12.19 (2019): 3721.

[3] Tu, Hao, et al. "Extreme fast charging of electric vehicles: A technology overview." *IEEE Transactions on Transportation Electrification* 5.4 (2019): 861-878.

[4] Un, Emre, and Ahmet M. Hava. "A near-state PWM method with reduced switching losses and reduced common-mode voltage for three-phase voltage source inverters." *IEEE Transactions on Industry Applications* 45.2 (2009): 782-793.

[5] Hou, Chung-Chuan, et al. "Common-mode voltage reduction pulsewidth modulation techniques for three-phase grid-connected converters." *IEEE transactions on Power Electronics* 28.4 (2012): 1971-1979..

[6] Hava, Ahmet M., and Emre Ün. "Performance analysis of reduced common-mode voltage PWM methods and comparison with standard PWM methods for three-phase voltage-source inverters." *IEEE Transactions on Power Electronics* 24.1 (2009): 241-252.

[7] Zhang, Haoran, et al. "Multilevel inverter modulation schemes to eliminate common-mode voltages." *IEEE transactions on industry applications* 36.6 (2000): 1645-1653.

[8] Huang, Yang, et al. "Analytical characterization of CM and DM performance of three-phase voltage-source inverters under various PWM patterns." *IEEE Transactions on Power Electronics* 36.4 (2020): 4091-4104.

[9] Zhang, Xuning, et al. "Filter design oriented EMI prediction model for DC-fed motor drive system using double fourier integral transformation method." *Proceedings of The 7th International Power Electronics and Motion Control Conference*. Vol. 2. IEEE, 2012.

[10] Sun, Yaxiu, Ruifeng Sun, and Junying Zhao. "Modeling of PWM drive motor system DM noise source." *2011 International Conference on Electrical and Control Engineering*. IEEE, 2011.

[11] Quan, Zhongyi, and Yun Wei Li. "Impact of PWM schemes on the common-mode voltage of interleaved three-phase two-level voltage source converters." *IEEE Transactions on Industrial Electronics* 66.2 (2018): 852-864.

[12] Celanovic, Nikola, and Dushan Boroyevich. "A fast space-vector modulation algorithm for multilevel three-phase converters." *IEEE transactions on industry applications* 37.2 (2001): 637-641.